Effects of microstructure on mixed-mode, high-cycle fatigue crack-growth thresholds in Ti-6Al-4V alloy

R. K. NALLA[1], J. P. CAMPBELL[2] and R. O. RITCHIE[1]

[1]*Department of Materials Science and Engineering, University of California, Berkeley, California 94720-1760, USA,* [2]*Metals Fabrication Division, General Motors, Troy, Michigan 48084, USA*

Received in final form 10 January 2002

ABSTRACT Effect of microstructure on mixed-mode (mode I + II), high-cycle fatigue thresholds in a Ti-6Al-4V alloy is reported over a range of crack sizes from tens of micrometers to in excess of several millimeters. Specifically, two microstructural conditions were examined—a fine-grained equiaxed bimodal structure (grain size ~20 μm) and a coarser lamellar structure (colony size ~500 μm). Studies were conducted over a range of mode-mixities, from pure mode I ($\Delta K_{II}/\Delta K_I = 0$) to nearly pure mode II ($\Delta K_{II}/\Delta K_I \sim 7.1$), at load ratios (minimum load/maximum load) between 0.1 and 0.8, with thresholds characterized in terms of the strain-energy release rate (ΔG) incorporating both tensile and shear-loading components. In the presence of through-thickness cracks—large (> 4 mm) compared to microstructural dimensions—significant effects of mode-mixity and load ratio were observed for both microstructures, with the lamellar alloy generally displaying the better resistance. However, these effects were substantially reduced if allowance was made for crack-tip shielding. Additionally, when thresholds were measured in the presence of cracks comparable to microstructural dimensions, specifically short (~200 μm) through-thickness cracks and microstructurally small (< 50 μm) surface cracks, where the influence of crack-tip shielding would be minimal, such effects were similarly markedly reduced. Moreover, small-crack ΔG_{TH} thresholds were some 50–90 times smaller than corresponding large crack values. Such effects are discussed in terms of the dominant role of mode I behaviour and the effects of microstructure (in relation to crack size) in promoting crack-tip shielding that arises from significant changes in the crack path in the two structures.

Keywords crack-tip shielding; fatigue thresholds; high-cycle fatigue; load ratio; microstructure; mixed mode; short cracks; Ti-6Al-4V; titanium.

INTRODUCTION

The control of failures owing to high-cycle fatigue (HCF) in turbine-engine components has been identified as one of the major challenges facing the readiness of the US Air Force fleet today.[1–3] In order to address this issue, a consortium of industrial, government and academic institutions has been charged with the task of modifying the existing design methodologies for improving the HCF reliability of these components.[4] One critical issue involves the effects of mixed-mode cyclic loads—that is, the presence of both tensile and shear loading—on the critical states of damage for such HCF failures. Indeed, there are many fatigue-critical locations within the turbine engine where such mixed-mode conditions exist—e.g. in the presence of fretting fatigue cracks in the blade–dovetail contact section.[5] The effective crack-driving force here can be considered to be a combination of the tensile (mode I) stress-intensity range, ΔK_I, the in-plane shear (mode II) stress-intensity range, ΔK_{II}, and/or the antiplane shear (mode III) stress-intensity range, ΔK_{III}. From the perspective of preventing HCF failures in turbine engines, it is critical that fatigue crack-growth thresholds are well-characterized for such loading conditions, as the extremely high cyclic frequencies (~1–2 kHz) involved can lead to very rapid

Correspondence: R. O. Ritchie, Department of Materials Science and Engineering, University of California, Berkeley, California 94720-1760, USA.
E-mail: RORitchie@LBL.gov

failures, with over three million cycles being accumulated in less than an hour. Moreover, the presence of mixed-mode loading conditions has been reported to reduce the mode I fatigue thresholds (e.g. Ref. [6]).

To date, studies on the HCF performance of engine alloys have largely focused on a bimodal microstructure of Ti-6Al-4V, an $\alpha+\beta$ alloy typically used in fan disks and compressors in the front, low-temperature stages of the engine. In the context of mixed-mode fatigue crack propagation, in addition to a few earlier reports on titanium (Ti) alloys in the literature,[7–9] Refs [10–12] provide the only results on mixed-mode thresholds in a bimodal Ti-6Al-4V alloy. In the present work, we seek to extend these earlier observations to a fully lamellar microstructure in the same alloy and to compare the relative merits of these two microstructures in mixed-mode fatigue. Specifically, the role of crack size in influencing mixed-mode fatigue thresholds is investigated through a study of large (>4 mm) and short ($\sim$200 μm) through-thickness cracks and microstructurally small (<50 μm) surface cracks, over a range of mode-mixities, from pure tension ($\Delta K_{II}/\Delta K_I = 0$) to predominantly shear ($\Delta K_{II}/\Delta K_I \sim 7.1$), and load ratios (ratio of minimum to maximum load), from $R = 0.1$–0.8.

BACKGROUND

The selection of a single microstructure in Ti-6Al-4V with optimal resistance to high-cycle fatigue is a complex task in view of the numerous factors influencing HCF failures. For example, coarse lamellar microstructures in many Ti alloys often possess superior toughness and fatigue crack-growth behaviour in the presence of large cracks as compared to the finer equiaxed microstructures; conversely, they can display lower high-cycle fatigue-endurance strengths and inferior small-crack growth behaviour (e.g. Refs [13–15]).

For the purpose of this study, two common microstructural conditions of Ti-6Al-4V are investigated—namely, the coarse-grained lamellar structures consisting of large β grains (diameter $\sim$1 mm) and a lamellar matrix of alternating α and β plates (produced by heat treatment in the high-temperature β-phase field and subsequent slow cooling into the $\alpha+\beta$ phase field) and the finer bimodal structures (produced by fast cooling from the β-phase field) with individual orientated α plates (plate width $\sim$1 μm). While lamellar structures are, in general, characterized by large α colonies (a packet of aligned α plates with same crystallographic orientation, about 200–400 μm in size), bimodal structures often consist of a low-volume fraction (typically $\sim$15–30%) of primary α grains ($\sim$20 μm in size) with colony-type lamellar matrix of alternating α and β plates within small β grains ($\sim$20–40 μm). For Ti-6Al-4V and other $\alpha+\beta$ Ti alloys, fatigue crack-propagation behaviour in such microstructures is well-characterized for pure mode I loading (e.g. Ref. [13–21]). Crack propagation in the α phase is generally parallel to the (0001) basal plane[21] and hence perpendicular to the orientation of the α lamellae.[22,23] The superior crack-growth resistance exhibited by lamellar structures has been attributed to this crystallographic nature of the crack trajectory, especially in the near-threshold regime. As the crack path differs from colony to colony, significant crack-path tortuosity results from out-of-plane deflection and secondary cracking, leading to enhanced crack-tip shielding.

Although similar explanations have been proposed for mixed-mode fatigue crack-propagation behaviour in Ti-6Al-4V,[12] there is little information on the role of microstructure in these alloys, or on how crack size may affect this role. The prime objective of the present work is to examine the effect of microstructure on such mixed-mode fatigue thresholds as a function of crack size, specifically through a study of bimodal and fully lamellar microstructures in Ti-6Al-4V.

EXPERIMENTAL PROCEDURES

Materials

The material investigated was a turbine-engine Ti-6Al-4V alloy, which originated as bar stock produced by Teledyne Titanium (Pittsburgh, PA, USA) specifically for the joint government-industry-academia HCF program. The composition (in wt.%) is given in Table 1. The original bar stock (63.5 mm in diameter) was sectioned into segments 400 mm long, preheated to 940 °C for 30 min and forged into $400 \times 150 \times 20$ mm plates. These plates were solution-treated at 925 °C for 1 h, fan air-cooled and then stabilized at 700 °C for 2 h.

Bimodal microstructure

The as-received microstructure of the alloy was in the bimodal condition (sometimes referred to as solution-treated and overaged, STOA), and consisted of colonies of equiaxed primary α and lamellar $\alpha+\beta$ (transformed β) (Fig. 1a). The proportion of primary α was 64.1% (standard deviation 6.6%), with an average grain size of $\sim$20 μm, slightly elongated in the longitudinal (L)

Table 1 Chemical composition of Ti-6Al-4V bar stock (in wt.%)[23]

Bar location	Ti	Al	V	Fe	O	N	H
Top	Bal.	6.27	4.19	0.20	0.18	0.012	0.0041
Bottom	Bal.	6.32	4.15	0.18	0.19	0.014	0.0041

direction of the forging.[24] Using differential thermal analysis, the β-transus temperature was measured to be 990–1005 °C.

Lamellar microstructure

For comparison, a fully lamellar microstructure was obtained by solution treating in a vacuum of 10^{-5}–10^{-6} mbar at 1005 °C (slightly above the β-transus) for 10–30 min (depending on the cross section), followed by a rapid quench (~100 °C min^{-1}) in high-purity helium (He); the quench rate was chosen in order to achieve a similar transformed β lath spacing as in the bimodal structure. The alloy was then stabilized at 700 °C for 2 h *in vacuo*, before slowly furnace cooling to ambient temperature. The resulting Widmanstätten microstructure (Fig. 1b) had an average prior-β grain size of ~1 mm, a colony size (parallel orientated α-phase lamellae) of ~500 μm, and an average α lamellae lath width of ~1–2 μm, similar to the interlamellar spacing of the transformed β in the bimodal microstructure.

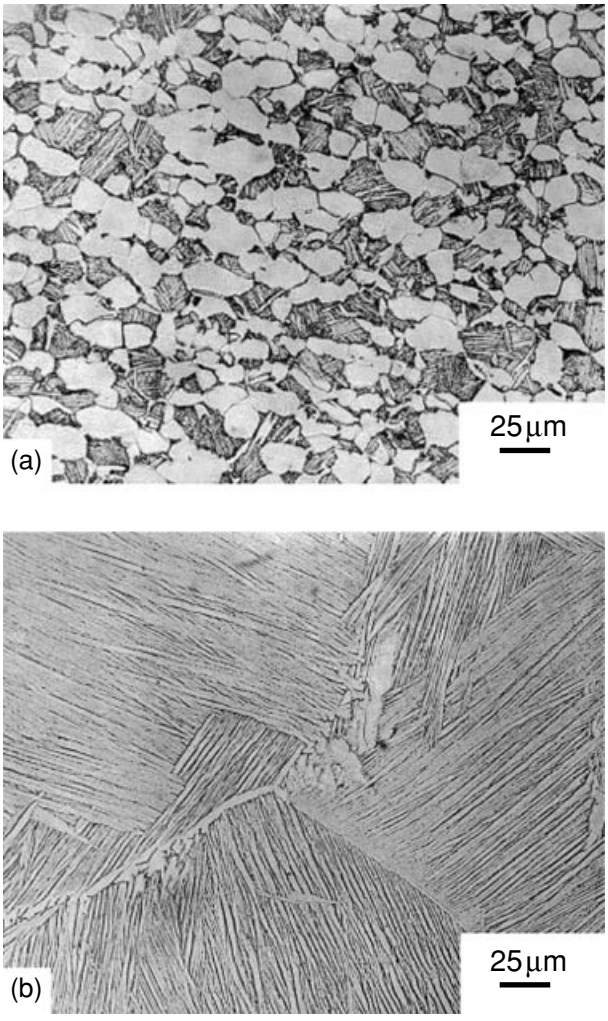

Fig. 1 Optical micrographs of the two microstructures of Ti-6Al-4V investigated: (a) bimodal (solution-treated and overaged, STOA) and (b) lamellar (β-annealed). Etched into ~10 sec in 5 parts 70% HNO_3, 10 parts 50% HF, 85 parts of H_2O.

Uniaxial tensile and toughness properties

Uniaxial tensile tests were conducted in both microstructures in the L-orientation using a strain rate of 5×10^{-4} s^{-1}; additional data for the bimodal microstructure were taken from Ref. [23]. Results in terms of the strength, ductility and toughness are listed in Table 2, and show that whereas the lamellar structure has somewhat higher strength, the bimodal structure exhibits over a factor of four higher ductility (owing to its smaller grain size that limits the effective slip length). However, despite its lower ductility, the lamellar microstructure has over 50% higher plane-strain fracture toughness.

Fatigue testing

Large through-thickness cracks

Large (> 4 mm) fatigue-threshold testing was performed in four-point bending, using 6 mm thick samples with inner and outer spans of 12.7 and 25.4 mm, respectively. Pure mode I tests were conducted using symmetric four-point bending. For mixed-mode loading, the mode II component of the loading was introduced using the asymmetric four-point bending (AFPB) configuration[25–28] where the mode-mixity ratio, $\Delta K_{II}/\Delta K_I$, can be varied using the offset, *s*, from the load line, as shown in Fig. 2. The values of mode I stress-intensity range, ΔK_I, and mode II stress-intensity range, ΔK_{II}, were determined from linear-elastic stress-intensity solutions for this geometry, recently developed by He and Hutchinson.[28]

Precracking was conducted in room temperature air in a near-identical manner for all large- and short-crack test samples in order to avoid any effect of precracking

Table 2 Uniaxial tensile and toughness properties of Ti-6Al-4V

Microstructure	Yield strength (MPa)	Ultimate tensile strength (MPa)	Reduction in area (%)	Fracture toughness K_{Ic} (MPa$\sqrt{m}$)
Bimodal	930	978	45	64
Lamellar	975	1055	10	100

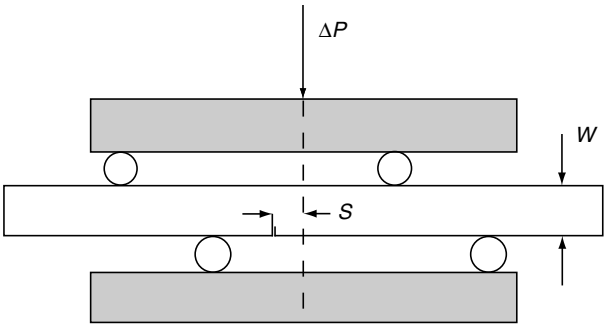

Fig. 2 The asymmetric four-point bend specimen. The offset, *s*, from the load line is used in order to control the degree of mode-mixity, $\Delta K_{II}/\Delta K_I$, and thereby the phase angle, $\beta = \tan^{-1}(\Delta K_{II}/\Delta K_I)$. This geometry is used for the mixed-mode large and short crack testing.

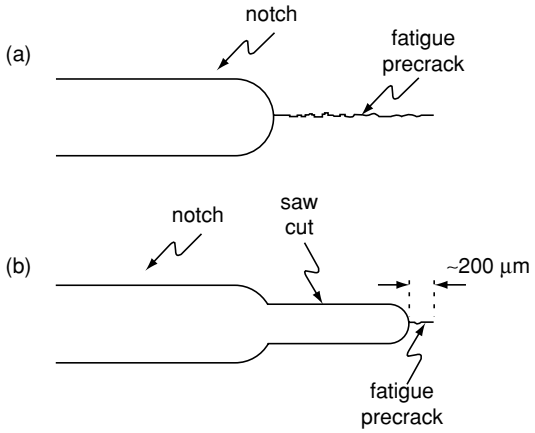

Fig. 3 The procedure used for removing the crack wake of a large crack in order to produce a short crack is illustrated.

technique on subsequent thresholds obtained. Specifically, fatigue cracks were grown from a 2 mm deep electrodeposition-machined (EDM) through-thickness notch in a symmetric four-point bending sample at a load ratio of 0.1 with a constant loading frequency. (This alloy is known to show little effect of frequency in room air, specifically over the range of 50–20 000 Hz in the bimodal structure[20] and 50–1000 Hz in the lamellar structure[22]). The surfaces of all samples required for crack-length observation were polished to a 0.05 μm finish, whereas the sides to be used to carry the load-bearing pins were ground to a 600 grit finish. As the effect of friction between the specimen and the roller-pin supports can substantially affect the stress-intensity values,[25] frictional effects were minimized at the pin-contact positions through the use of a high-pressure MoS_2 grease. The final precrack length thus achieved was 4.50 ± 0.25 mm at near-threshold ΔK_I values of 4.8 ± 0.5 and 6.8 ± 0.5 MPa$\sqrt{\text{m}}$, respectively, for the bimodal and lamellar microstructures.

For large crack (> 4 mm) tests, mode-mixities were varied from $\Delta K_{II}/\Delta K_I = 0$ (pure mode I) to $\Delta K_{II}/\Delta K_I \sim 7.1$ (nearly pure mode II), representing a change in phase angle, $\beta = \tan^{-1}(\Delta K_{II}/\Delta K_I)$, from 0 to 82°. Load ratios were varied from $R = 0.1$–0.8. Tests involving cycling precracked specimens at a specified mode-mixity were performed in the following way: if no crack growth was observed (using an optical microscope) after 2×10^6 cycles, either ΔK_I or ΔK_{II} was increased by ~0.25 MPa$\sqrt{\text{m}}$ (with the other being increased accordingly to maintain the mode-mixity) and the procedure repeated. In this way, a 'growth/no growth' condition bounding the actual threshold was obtained. The crack extension defining 'growth' was taken to be of the order of the characteristic microstructural dimension—that is, ~20 μm for the bimodal structure and ~500 μm for the lamellar structure, yielding threshold growth rates of 10^{-10}–10^{-11}m cycle^{-1}. The larger 'growth' condition for the lamellar structure also served to ensure adequate sampling of the relatively heterogeneous microstructure.

The magnitude of the crack-tip shielding—used for computing the effective (near-tip) crack-driving force in both modes I and II—was characterized using a recently developed compliance-based technique for both tensile opening and shear-type loading, using two displacement gauges mounted near the crack tip to measure opening and shear displacements. As described, in detail, in Ref. [11], the distinction between the contributions to shielding in modes I and II was achieved by examining separate load-displacement curves using these two crack-tip gauges. Mode I shielding, in the form of crack closure, was determined from the compliance curve for the opening displacements from the first deviation from linearity on unloading, whereas mode II shielding, in the form of crack-surface interference via asperity rubbing and interlock, was determined in an analogous fashion from the compliance curve for shear displacements.

Short through-thickness cracks

In order to examine the influence of crack size on mixed-mode fatigue thresholds, the behaviour of large (> 4 mm) through-thickness cracks was compared with those of short (~200 μm) through-thickness cracks and small (< 50 μm) surface cracks. The distinction and relevance of these types of flaws are discussed, in detail, in Appendix A.

Mixed-mode threshold tests on the short cracks were measured on 6–12 mm thick four-point bend bars, using procedures identical to those described above for large cracks, except that the precrack wake was carefully machined away to within ~200 μm of the crack tip using a

slow-speed diamond saw (Fig. 3). The rationale for this procedure of removing most of the crack wake was to limit the effect of crack-tip shielding by minimizing the occurrence of any premature contact of the crack faces during unloading. However, as the short cracks were through-thickness, they still 'sampled' the continuum microstructure—that is, typically between 30 and 300 grains. Thresholds were measured in both microstructures at load ratios of $R = 0.1$–0.8 for mode-mixities of $\Delta K_{II}/\Delta K_I = 0$ to $\Delta K_{II}/\Delta K_I \sim 7.1$ (i.e. $\beta = 0$–82°).

Small surface cracks

Mixed-mode thresholds for microstructurally small surface cracks were performed using an inclined-crack technique. Wide bend bars (16–25 mm width, 5 mm thickness) were machined in the L–T orientation, with the surfaces required for observation polished to a 0.05 μm finish, and the sides used to carry the load-bearing pins ground to a 600 grit finish. A stress-relief treatment of 2 h at 695 °C *in vacuo* was used in order to minimize any residual stresses from machining and specimen preparation. A 'precrack' was naturally initiated at the stress of $\sigma_{max} = 750$ MPa—that is, ~80% of yield strength—using standard three-point bending (with a load ratio of 0.1 and a frequency of 50 Hz). In order to enable measurement of the small-crack thresholds, a bend bar was carefully machined out from the original precracked wide bar with the crack inclined at the desired angle (Fig. 4). This sample was subsequently subjected to four-point bending by cycling at a load ratio of 0.1. If no growth (defined as a total crack extension of less than 20 μm per 2×10^6 cycles on both ends of the surface crack) was observed, the maximum load (and proportionately the minimum load) was increased by 111 N and the above-mentioned procedure was repeated. Thresholds were thus again determined using a 'growth/no growth' criterion, but for the bimodal microstructure only. The inclined-crack technique could not be usefully employed for the lamellar microstructure as a result of the highly deflected nature of fatigue cracking in this structure.

Linear-elastic solutions for the stress intensities associated with the small, semielliptical surface cracks under mixed-mode loading were taken from two sources. On

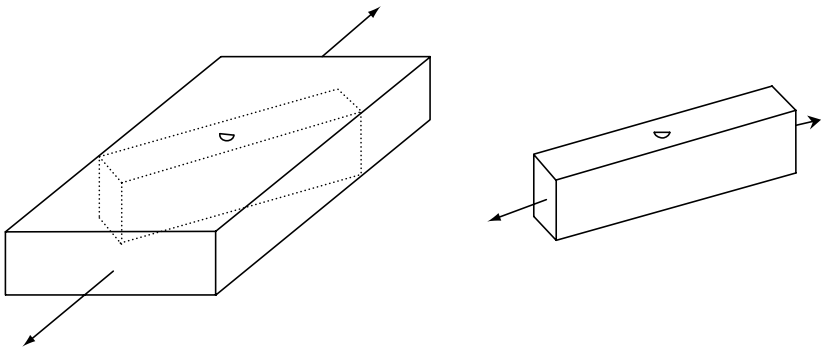

(a) **wide bend bar specimen** (b) **small 'inclined crack' specimen**

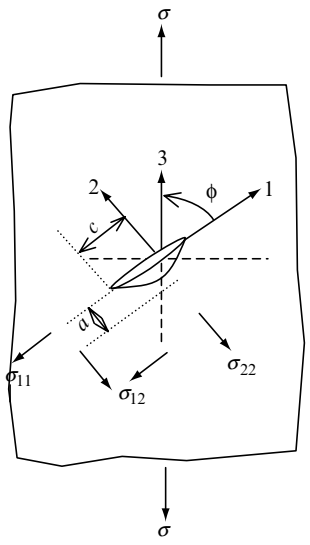

(c) **mixed-mode small crack testing**

Fig. 4 Schematic showing the procedures utilized for obtaining the small 'inclined crack' specimen. (a) The dotted lines outline the small-crack test sample to be machined at the desired angle of inclination, ϕ from the original wide bend bar. The nominal direction of loading for crack initiation is also shown. (b) The final 'inclined crack' specimen is illustrated. (c) Schematic of the inclined semielliptical surface crack configuration used for the microstructurally small-crack testing. The tensile loading component, σ_{22}, induces the mode I contribution, whereas the shear-loading component, σ_{12}, induces the mode II and mode III components.

the basis that the crack plane was normal to the specimen surface, the mode I component of the stress intensity, K_I, was computed from the well-known Newman–Raju solution:[29]

$$K_I = (\sigma_t + H\sigma_b) \sqrt{\pi \frac{a}{Q}} F\left(\frac{a}{t}, \frac{a}{c}, \frac{c}{b}, \theta\right) \quad (1)$$

where σ_t is the remote uniform tension stress and σ_b is the remote uniform outer-fibre bending stress. The geometrical factors—H, Q and F—are evaluated from: the crack depth, a; the crack half-length, c; the specimen thickness, t; the specimen half-width, b; and the angular position along the crack front, θ, as described in detail in Ref. [29].

The mode II component, K_{II}, conversely, was computed from the newly derived He–Hutchinson solution[30] for elliptical surface cracks under mixed-mode loading:

$$K_{II} = \chi \sigma_{12} \sqrt{\pi a} \quad (2)$$

where χ is a numerical factor determined from Ref. [30]; σ_{12} is the shear component of the loading and a is the crack depth. It should be noted here that a three-dimensional corner singularity exists in the solution at the point where the crack intersects with the free surface. However, for the purpose of this study, this is ignored because errors caused by such an assumption are negligible. Moreover, as one moves along the crack front to the interior, the magnitude of the mode II contribution decreases with that of mode III increasing till the point of deepest penetration of the crack is reached.

The applied load/stress on the inclined crack (Fig. 4c) was resolved trigonometrically into tensile and shear components. The tensile component was used for determining ΔK_I, using Ref. [29] and the shear component for ΔK_{II} and ΔK_{III}, using Ref. [30]. As the exact shape of such small surface cracks and the variation in this aspect ratio with crack extension clearly can have an important effect on the crack-driving force and hence the crack-growth behaviour,[31,32] crack shapes (Fig. 4)—in the form of the depth-to-surface length ratio, $a/2c$—were determined by postfracture observations; the typical aspect ratio was $a/2c \sim 0.45$.

The use of linear-elastic stress-intensity solutions for characterizing the driving forces for the small cracks is justified on the basis of the small cyclic plastic-zone sizes in relation to crack size. For example, for the smallest crack sizes of $\sim$1 μm, where the ΔK_I thresholds are $\sim$1 MPa m^{-1}, plastic-zone size (estimated as $r_y \sim 1/2\pi (\Delta K_I/\sigma_y)^2$ where σ_y is the yield strength) are on the order of 100 nm. As this is roughly one-tenth of the crack size, it is deemed reasonable to conclude that small-scale yielding conditions prevail.

RESULTS

Large-crack behaviour

Effect of load ratio and mode-mixity

Large crack thresholds for the bimodal and lamellar microstructures under mode I + II loading are shown in Fig. 5 in the form of mixed-mode threshold envelopes, where the mode II threshold stress-intensity range, $\Delta K_{II,TH}$, is plotted as a function of the corresponding mode I threshold stress-intensity range, $\Delta K_{I,TH}$ (note that each threshold is represented by two data points, which indicate the 'growth' and 'no growth' conditions). The phase angles investigated were 0, 26, 62 and 82° for load ratios of 0.1 and 0.5, and 0, 26 and 62° at a load ratio of 0.8 for both structures. Based on these results, the following observations can be made:

- Akin to behaviour in most metallic alloys (e.g. Refs [8–9,33–35]), a reduction in the fatigue threshold values is clearly evident for both microstructures with increasing load ratio. The slight increase in the mode I threshold, $\Delta K_{I,TH}$, with increasing mode-mixity at low phase angles, observed in the present data at phase angles between 0 and 26°, has been attributed to the effect of mode I/mode II crack-tip shielding.[10–12]
- The mode I threshold, $\Delta K_{I,TH}$, clearly decreases with increasing mode-mixity. However, if a more appropriate driving force—incorporating both mode I and mode II components—is used in order to characterize the threshold, specifically the range in strain-energy release rate, $\Delta G = (\Delta(K_I^2 + \Delta K_{II}^2)/E'$ where $E' = E$ (E is Young's modulus) in plane stress and $E/(1\text{-}\nu^2)$ in plane strain (ν is Poisson's ratio), then there is a progressive increase in the mixed-mode ΔG_{TH} fatigue threshold with increasing mode-mixity in both microstructures for all load ratios studied (Fig. 6). This can alternatively be represented in terms of an equivalent stress-intensity factor range, $\Delta K_{eq,TH} = (\Delta G_{TH} E')^{1/2}$, which is also plotted in Fig. 6. Note that in this and all subsequent figures, threshold values are represented by a single data point showing the average value of the 'growth/no growth' conditions. An alternative means of calculating the mixed-mode thresholds is briefly described in Appendix B.
- From the perspective of thresholds for high-cycle fatigue in Ti-6Al-4V, the results in Fig. 6 strongly imply that despite the presence of mixed-mode loading, the mode I threshold, defined in terms of the strain-energy release rate, ΔG, for cracks large compared to microstructural dimensions, represents a *worst-case* condition for the onset of fatigue crack growth under mode I + II loading for both microstructures.
- Though both microstructures showed mixed-mode ΔG_{TH} thresholds that increased substantially with

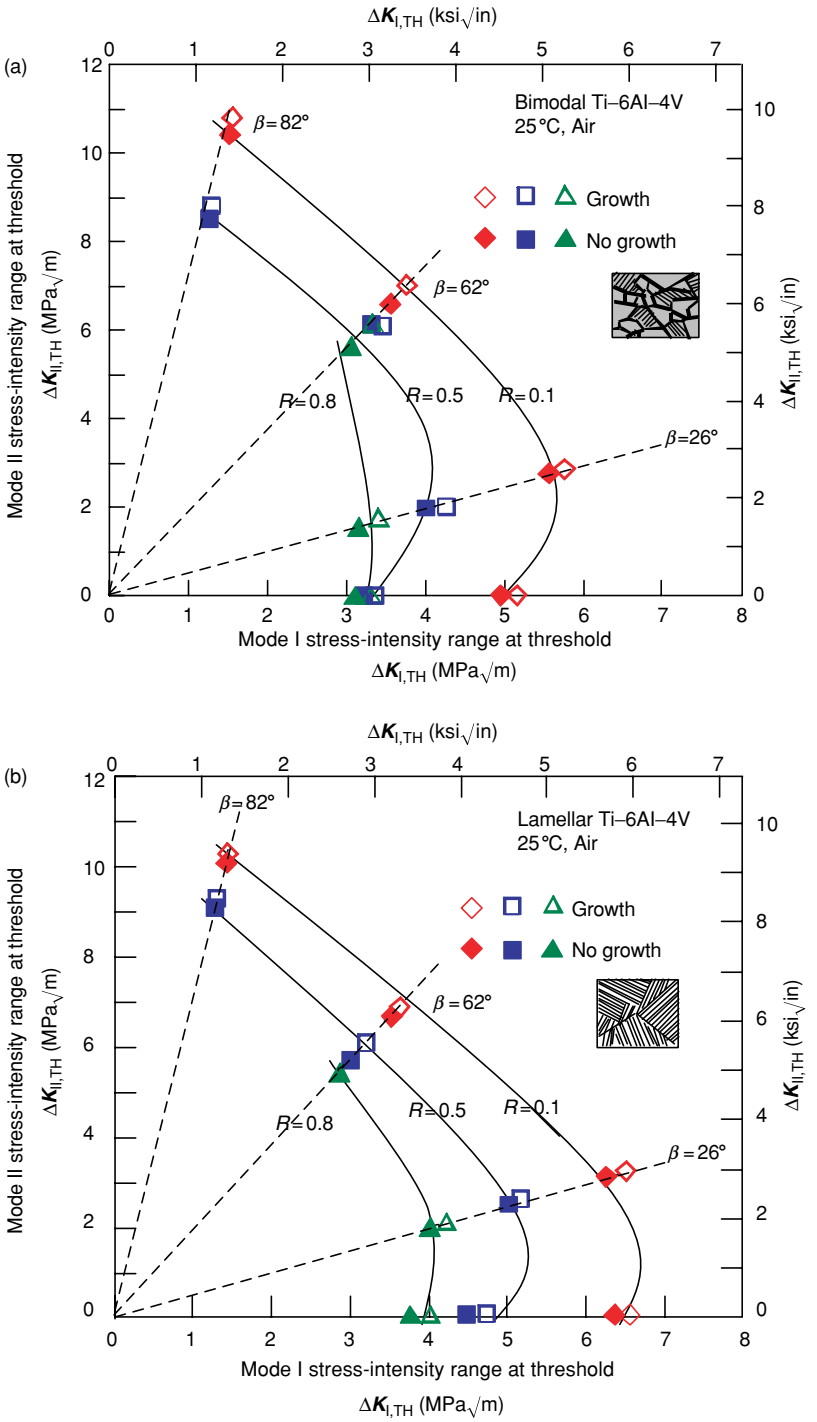

Fig. 5 Mixed-mode threshold envelopes for large (> 4 mm) through-thickness cracks in the (a) bimodal and (b) lamellar microstructures. Note that the lamellar structure shows superior resistance to crack propagation, particularly at the lower phase angles.

increasing mode-mixity, in general the lamellar structure was observed to exhibit the higher threshold values. However, the better fatigue resistance of the lamellar structure was markedly reduced at high mode-mixities, as is evident from the large-crack threshold values listed in Table 3 (the difference between the thresholds for the two microstructures is included in parentheses for the purpose of comparison). Clearly, the superior fatigue crack-growth properties of the lamellar structure at low mode-mixities ($\beta = 0$ and 26°) are nearly eliminated, or in some cases reversed, when significant mode II loading is present ($\beta = 62$ and 82°).

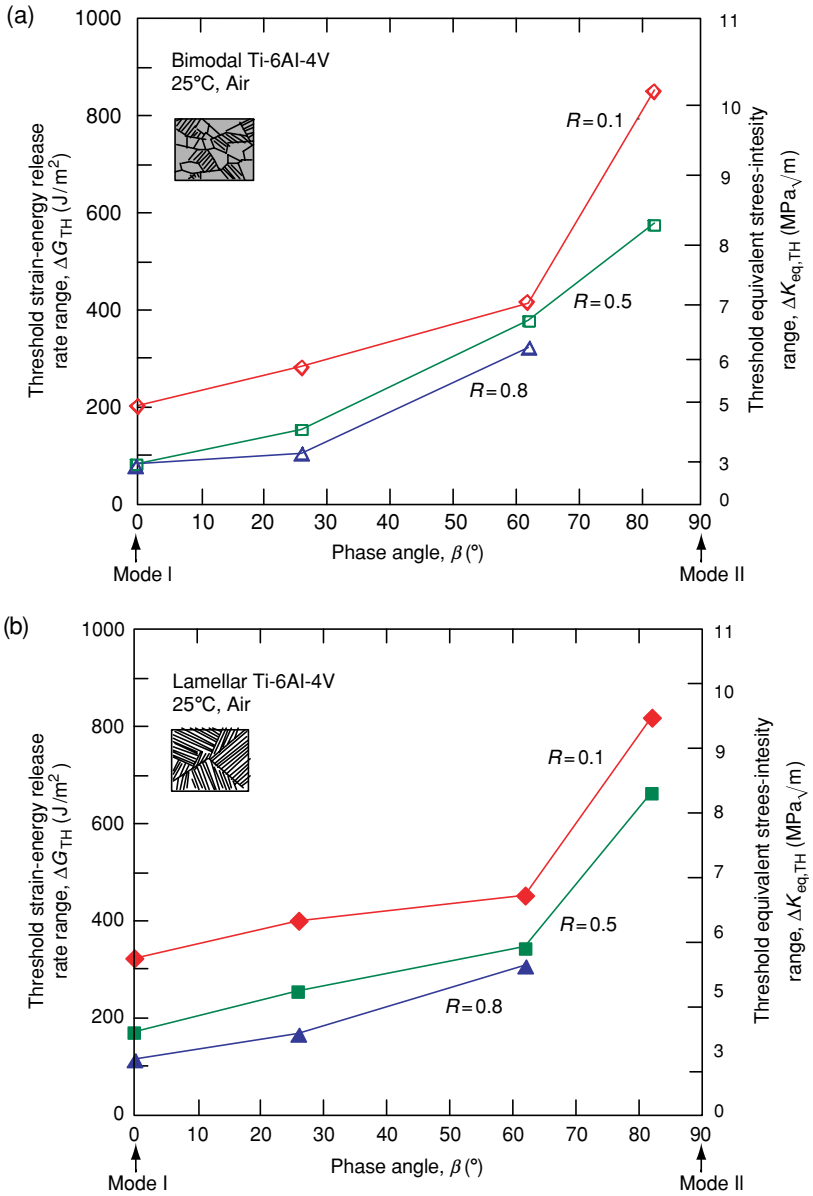

Fig. 6 The threshold strain-energy release rate, ΔG_{TH}, is plotted as a function of phase angle, β, for the (a) bimodal and (b) lamellar microstructure for large cracks subjected to mixed-mode loading at $R = 0.1$, 0.5 and 0.8. Equivalent stress-intensity ranges at threshold, $\Delta K_{eq,TH}$, for both microstructures are also shown. The lamellar microstructure, in general, shows superior resistance to fatigue-crack propagation, although the difference is reduced at high mode-mixities.

Role of crack-tip shielding

As discussed in Refs. [10,11] for the bimodal structure, the increase in the large-crack mixed-mode thresholds with increasing mode-mixity can be directly related to an increased role of mode I and mode II crack-tip shielding, associated with, respectively, crack closure and sliding crack interference (friction and interlock of crack-surface asperities). This can be appreciated by quantifying the magnitude of such shielding in order to determine a mixed-mode, effective strain-energy release rate, ΔG_{eff}, and then 'correcting' the large-crack threshold data in Fig. 6 for such shielding by characterizing in terms of ΔG_{eff}.

The effective (near-tip) strain-energy release rate, ΔG_{eff}, can be defined as $(\Delta K_{I,eff}^2 + \Delta K_{II,eff}^2)/E'$, where $\Delta K_{I,eff}$ is the effective stress-intensity range in mode I and $\Delta K_{II,eff}$ is the corresponding effective stress-intensity range in mode II. In the present work, $\Delta K_{I,eff}$ was determined in the usual fashion used in order to measure crack closure—that is, in terms of $K_{I,max}$–K_{cl}, where K_{cl} is the closure stress intensity defined at the first deviation from linearity of the crack-tip load-displacement curve on unloading. On the other hand, $\Delta K_{II,eff}$ was measured as the difference between the near-tip maximum and minimum mode II stress intensities in the fatigue cycle. The near-tip mode II stress-intensity range differs from the applied driving force as a result of the presence of shear-induced fracture-surface asperity contact and interlock. Further details on the determination of $\Delta K_{I,eff}$ and the estimation of $\Delta K_{II,eff}$ using compliance-based techniques can be found in Ref. [11].

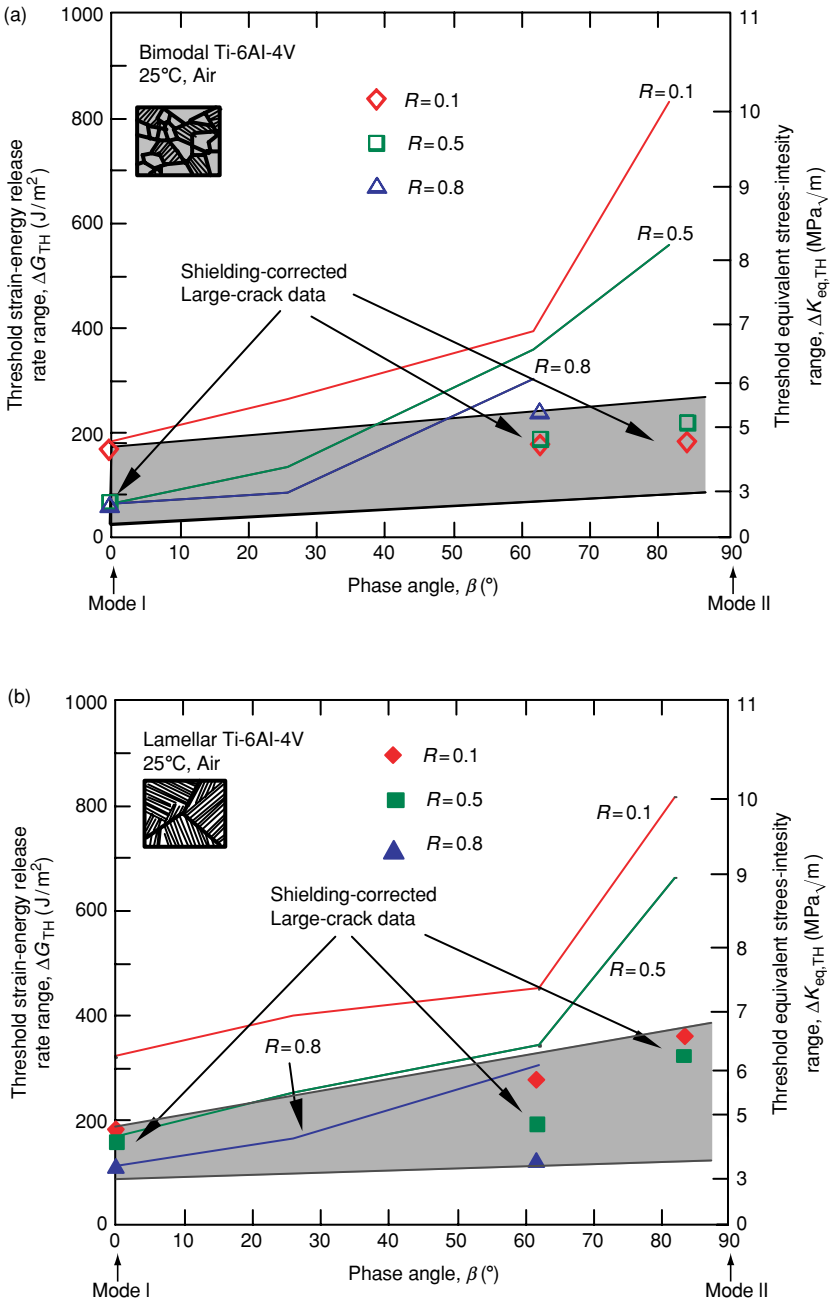

Fig. 7 The threshold strain-energy release rate, ΔG_{TH}, is plotted as a function of phase angle, β, for the (a) bimodal and (b) lamellar microstructure for large cracks subjected to mixed-mode loading at $R = 0.1$, 0.5 and 0.8. Results from Fig. 6 are compared with the $\Delta G_{TH,eff}$ values which have been corrected for crack-tip shielding. Note the relative absence of any effect of mode-mixity and/or load ratio on the shielding-corrected thresholds.

By so characterizing the driving force in terms of ΔG_{eff} by subtracting out the contributions from crack-tip shielding (individual ΔK_I and ΔK_{II} values are listed in Tables 4 and 5), the effect of mode-mixity on the threshold is found to be greatly reduced for both microstructures. This can be seen in Fig. 7 where the 'shielding-corrected' $\Delta G_{eff,TH}$ thresholds (plotted as hatched regions) are compared with the 'uncorrected' data of Fig. 6. Several points are worthy of note:

- The shielding-corrected $\Delta G_{eff,TH}$ threshold values are substantially smaller (by as much as a factor of four) than the uncorrected ΔG_{TH} values, especially at high phase angles.
- Mixed-mode threshold values are essentially independent of both load ratio and mode-mixity. While it is generally appreciated that the effect of load ratio on mode I threshold values is largely associated with crack closure (e.g. Refs [19,20]), these results confirm earlier reports for the bimodal structure[10,11] that the effect of mode-mixity in increasing the ΔG_{TH} threshold in Ti-6Al-4V can be principally attributed to an increase in crack-tip shielding (mainly from enhanced crack-surface interference).

Table 3 Fatigue threshold values for large fatigue cracks in Ti-6Al-4V

Mode-mixity	ΔG_{TH} (J m^{-2})			$\Delta K_{eq,TH}$ (MPa$\sqrt{m}$)		
	$R = 0.1$	$R = 0.5$	$R = 0.8$	$R = 0.1$	$R = 0.5$	$R = 0.8$
Bimodal microstructure:						
0°	200	80	80	4.9	3.1	3.1
26°	280	150	100	5.8	4.3	3.5
62°	410	375	320	7.0	6.7	6.2
82°	850	575	–	10.1	8.3	–
Lamellar microstructure*:						
0°	320 (+60%)	170 (+113%)	110 (+38%)	6.2	4.5	3.6
26°	395 (+41%)	255 (+70%)	165 (+65%)	6.9	5.5	4.5
62°	450 (+10%)	345 (−8%)	305 (−5%)	7.4	6.5	6.1
82°	815 (−4%)	660 (+15%)	–	9.9	8.9	–

*The numbers in parentheses indicate the difference between the magnitudes of the ΔG_{TH} threshold of the lamellar structure as compared to the bimodal threshold.

Table 4 Comparison of the applied and shielding-corrected mode I stress-intensity ranges

Load ratio	Mode-mixity	$\Delta K_{I,TH}$ (MPa$\sqrt{m}$)	$\Delta K_{I,TH,eff}$ (MPa$\sqrt{m}$)	Reduction in ΔK_I(MPa$\sqrt{m}$)*
Bimodal microstructure:				
0.1	0°	5.0	4.7	0.3 (6%)
	62°	3.6	2.8	0.8 (22%)
	82°	1.5	0.6	0.9 (60%)
0.5	0°	3.3	3.3	0.0 (0%)
	62°	3.3	1.7	1.6 (48%)
	82°	1.2	0.0	1.2 (100%)
0.8	0°	3.2	3.2	0.0 (0%)
	62°	3.1	2.3	0.8 (26%)
Lamellar microstructure:				
0.1	0°	6.5	4.6	1.9 (29%)
	62°	3.6	2.2	1.4 (39%)
	82°	1.4	0.8	0.6 (43%)
0.5	0°	4.6	4.3	0.3 (7%)
	62°	3.1	2.8	0.3 (10%)
	82°	1.3	0.5	0.8 (62%)
0.8	0°	3.9	3.7	0.2 (5%)
	62°	2.9	2.5	0.4 (14%)

*The numbers in parentheses indicate the percentage reduction in ΔK_I owing to correction for crack-tip shielding.

- The superior mixed-mode fatigue threshold properties of the lamellar microstructure are substantially reduced when results are plotted in terms of ΔG_{eff}, suggesting that this is also associated with higher levels of crack-tip shielding. This is consistent with the significantly more tortuous crack paths observed in the lamellar structure, which would promote crack-surface interference, as discussed in the following section.

Table 5 Comparison of the applied and shielding-corrected mode II stress-intensity ranges

Load ratio	Mode-mixity	$\Delta K_{II,TH}$ (MPa$\sqrt{m}$)	$\Delta K_{II,TH,eff}$ (MPa$\sqrt{m}$)	Reduction in ΔK_{II} (MPa$\sqrt{m}$)*
Bimodal microstructure:				
0.1	62°	6.5	3.9	2.6 (40%)
	82°	10.4	4.8	5.6 (54%)
0.5	62°	6.0	4.6	1.4 (23%)
	82°	8.6	5.3	3.3 (38%)
0.8	62°	5.6	5.0	0.6 (11%)
Lamellar microstructure:				
0.1	62°	6.7	5.2	1.5 (22%)
	82°	10.1	6.6	3.5 (35%)
0.5	62°	5.8	3.8	2.0 (35%)
	82°	9.1	6.2	2.9 (32%)
0.8	62°	5.5	2.9	2.6 (47%)

*The numbers in parentheses indicate the percentage reduction in ΔK_{II} owing to correction for crack-tip shielding.

Crack path and fractography

Akin to fatigue crack-growth behaviour in pure mode I in the presence of large cracks,[22] the lamellar microstructure displays superior crack-growth resistance under mixed-mode loading compared to the bimodal structure. This can be attributed to the large degree of crack-path deflection, bifurcation and secondary crack formation associated with crack growth in the lamellar structure. Typical crack paths are illustrated in Fig. 8 for both microstructures, and show the pure mode I precrack (grown at $R = 0.1$) and subsequent crack growth under

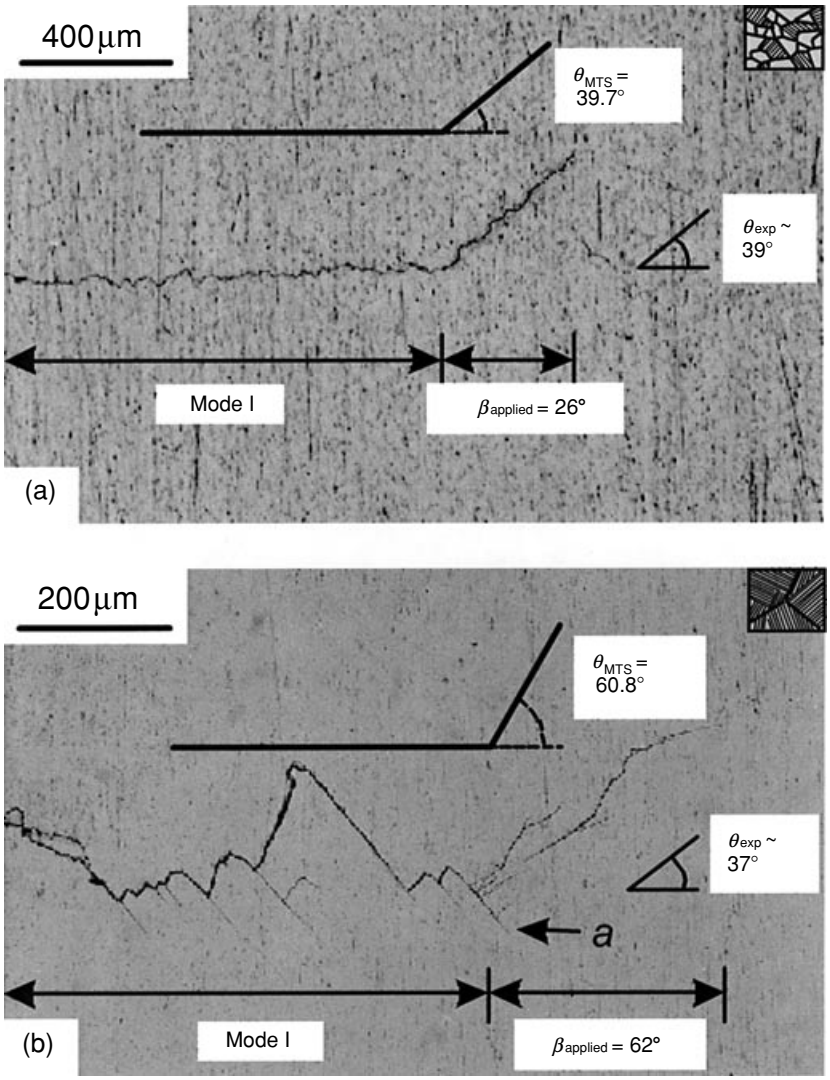

Fig. 8 Typical fatigue crack profiles are compared for the (a) bimodal ($R = 0.8$, $\beta = 26^\circ$, $\Delta G_{TH} = 100\,J\,m^{-2}$) and (b) lamellar ($R = 0.1$, $\beta = 62^\circ$, $\Delta G_{TH} = 450\,J\,m^{-2}$) microstructures. Optical micrographs show both the mode I fatigue precrack and the region of deflected crack growth following the application of cyclic mixed-mode loading. Measured crack deflection angles, θ_{exp}, are compared with those predicted by the path of maximum tangential stress, θ_{MTS} (see Ref. [12]).

mixed-mode loading (at $R = 0.8$ with $\Delta K_{II}/\Delta K_I = 0.5$ for the bimodal structure and at $R = 0.1$ with $\Delta K_{II}/\Delta K_I = 1.9$ for the lamellar structure). There is clearly a substantial difference between the trajectories of cracks in the two structures. This is evident (i) in the crack path especially during mode I crack growth, where the lamellar structure shows substantially higher tortuosity owing to interaction of the crack with the much coarser lamellar microstructure—with characteristic length scales of ~500 μm—and (ii) in the crack direction at the onset of mixed-mode loading, as discussed below.

The crack-path direction is determined through a competition between the maximum crack-driving force and the weakest microstructural path. In fine-scale, homogeneous microstructures, such as the bimodal microstructure (where characteristic length scales are ~20 μm), the crack-driving force becomes the dominant factor. For nominally elastic conditions, the path of a growing fatigue crack will change in response to a change in the applied phase angle, so that a pure mode I near-tip condition is maintained—that is, the crack tip follows a path dictated by either a zero mode II stress intensity ($K_{II} = 0$), maximum tangential stress (MTS), or maximum strain-energy release rate, G_{max}[36,37]— all criteria that yield essentially the same crack-path predictions (except at very high phase angles). Accordingly, cracks in the bimodal structure deflect under mixed-mode loading to follow a mode I path, as illustrated in Fig. 8a where the crack deviates almost exactly along the path of maximum tangential stress. For the coarse lamellar structure, conversely, Fig. 8b shows that the crack does not deflect along the maximum tangential stress direction at the onset of the mixed-mode loading; here, the characteristic microstructural dimensions are far larger, so that the crack path *on this scale of observation* cannot be described by continuum notions and is markedly influenced by microstructure. Similar deviations from predicted mode I crack paths under mixed-mode loading have

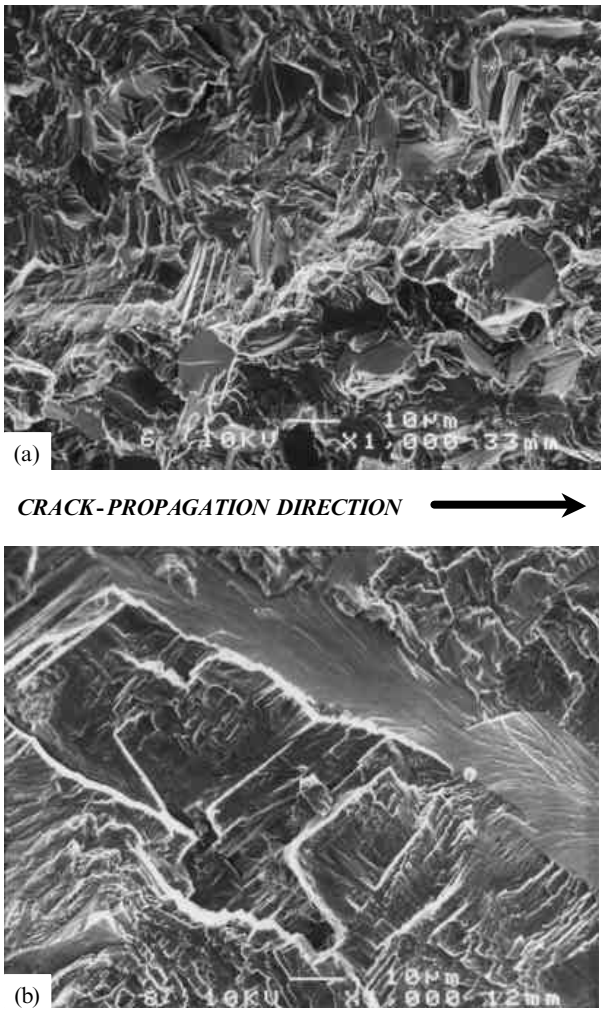

Fig. 9 Typical fractography for mixed-mode fatigue crack growth in the (a) bimodal ($\Delta G_{TH} = 410\,J\,m^{-2}$) and (b) lamellar microstructures ($\Delta G_{TH} = 450\,J\,m^{-2}$). Both specimens were tested at load ratio, $R = 0.1$, and phase angle, $\beta = 62^{\circ}$. The much coarser length scales involved for the lamellar structure are evident.

been observed for coarse-grained lamellar microstructures in titanium aluminide intermetallics, where fatigue cracks can follow a preferential interlamellar path within a single large colony.[38]

All these factors result in substantially rougher fracture surfaces (Fig. 9) in the lamellar microstructure, which *with large cracks* promotes both mode I crack closure, through premature crack-surface asperity contact on unloading, and mode II crack-surface interference, through enhanced asperity rubbing and interlocking within the sliding crack faces. Measurements of the magnitude of such closure and surface interference, listed in Tables 4 and 5, provide experimental confirmation of the more significant role of crack-tip shielding in the coarser lamellar structure; this provides the main reason why this microstructure displays superior resistance to (large crack) fatigue crack propagation, with higher measured fatigue threshold values under both pure mode I and mixed-mode loading conditions.

Short-crack behaviour

Corresponding mixed-mode ΔG_{TH} thresholds for short ($\sim$200 μm) through-thickness cracks in the bimodal and lamellar structures (at $\beta = 0$–82° and $R = 0.1$–0.8) are plotted as a function of the phase angle in Fig. 10; results are compared with the corresponding thresholds (both uncorrected and shielding-corrected) for large cracks from Fig. 7. As noted above, the effect of crack-tip shielding in the crack wake is particularly significant in the presence of shear loading owing to crack-surface friction and interlocking of asperities.[39–41] Consequently, owing to the minimal role of crack-tip shielding associated with cracks of limited wake, measured short crack ΔG_{TH} thresholds were:

- substantially lower than the corresponding large-crack values (similar to results for mode I thresholds[22]),
- essentially insensitive to the degree of mode-mixity, in marked contrast to the large crack thresholds, and
- relatively insensitive to the load ratio, again in contrast to large crack results.

Moreover, the short-crack threshold values, which are listed in Table 6, were observed to lie within the scatterband for shielding-corrected large cracks, again indicating that, similar to observations under pure mode I conditions, the limited effect of shielding for short cracks is responsible for their lower threshold values.

With respect to the role of microstructure, the distinction between the bimodal and lamellar microstructures in terms of the mixed-mode crack-growth resistance is substantially reduced for short cracks compared to that for large cracks. This again implies that the primary effect of microstructure on mixed-mode fatigue thresholds in Ti-6Al-4V arises through the mechanism of crack-tip shielding. Where the role of such shielding is restricted, as in the case of short cracks with limited wake, differences in fatigue resistance between the bimodal and lamellar structures become much less significant. Analogous behaviour can be seen under mode I loading where the superior fatigue crack-growth properties of the lamellar structure are lost at high load ratios, where the effect of crack closure becomes insignificant; once again, the primary role of microstructure occurs through mechanisms of crack-tip shielding.[22]

Small-crack behaviour

A more realistic flaw—in terms of what is most commonly encountered in real structures—is that of the

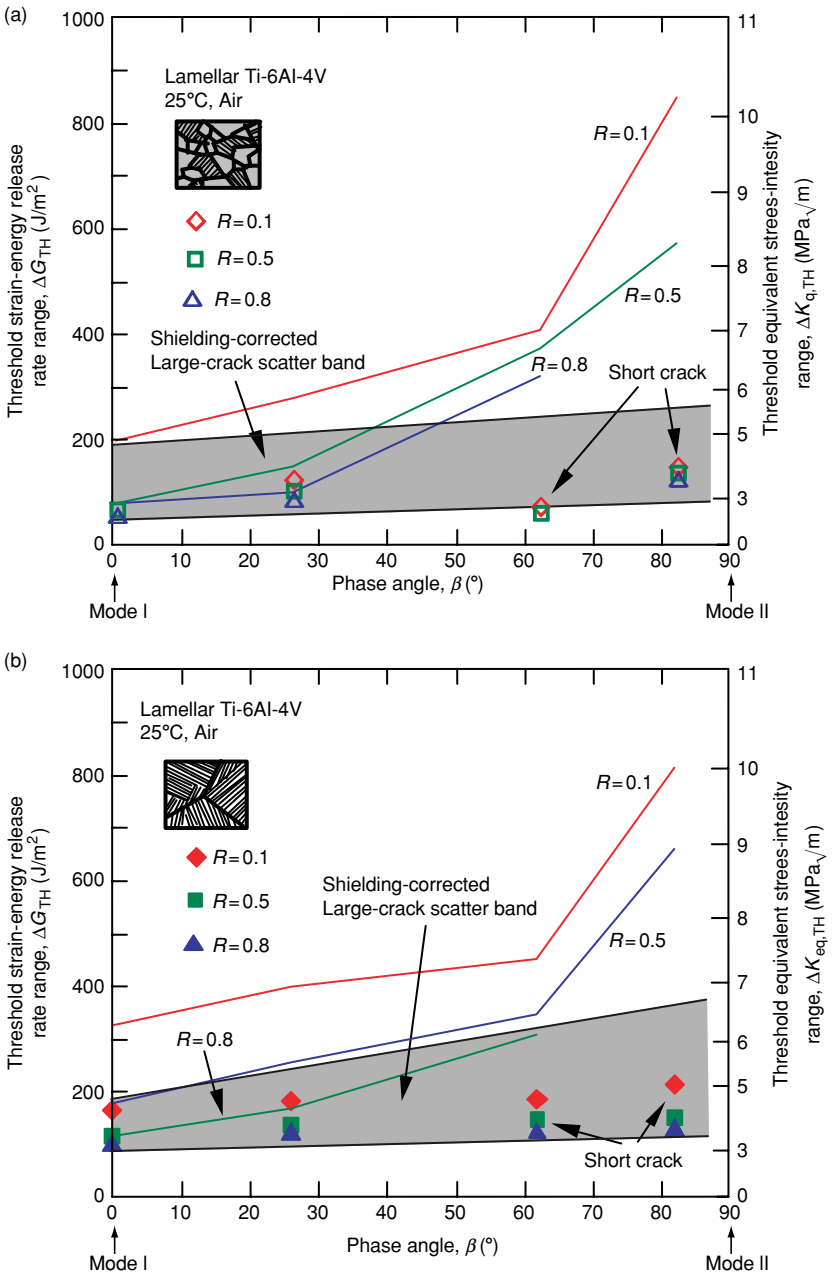

Fig. 10 Variation in mixed-mode thresholds, ΔG_{TH}, as a function of phase angle, β, in (a) bimodal and (b) lamellar structures. Shown are results at three load ratios for large (> 4 mm) cracks, before and after 'correcting' for crack-tip shielding, and for short (~200 μm) through-thickness cracks. The lamellar microstructure shows somewhat superior resistance to crack propagation in the short crack regime.

small, semielliptical surface crack, which is small in all dimensions. Like short cracks, such cracks experience a minimal effect of crack-tip shielding owing to their limited wake. In the present study on Ti-6Al-4V, mode I ΔG_{TH} thresholds for such microstructurally small (< 50 μm) cracks in both the bimodal and lamellar structures are compared with corresponding mixed-mode large-crack data in Fig. 11. Threshold values for the small cracks are clearly much smaller than the corresponding values for large cracks. Indeed, small cracks are observed to propagate at threshold levels above $\Delta G_{TH} = 8.3\,J\,m^{-2}$ ($\Delta K_{I,TH} \sim 1\,MPa\sqrt{m}$), whereas the *worst-case* ΔG threshold for large cracks, namely $\Delta G_{TH} = 29.9\,J\,m^{-2}$ ($\Delta K_{I,TH} \sim 1.9\,MPa\sqrt{m}$), is a factor of three larger.

Microstructurally, again it is clear that whereas the lamellar structure has superior large-crack threshold properties, this is not apparent in the presence of small cracks where the mode I thresholds are almost identical. Even the subsequent small-crack growth rates, shown as a function of ΔK_I in Fig. 12 from a parallel study on the effects of foreign-object damage on high-cycle fatigue in Ti-6Al-4V[42] reveal few differences in the behaviour of the bimodal and lamellar microstructures—observations

which can be related to the minimal role of crack-tip shielding with cracks of limited wake.

However, the behaviour of the small surface crack is different from that of the short (and large) through-thickness crack in the manner in which it statistically 'samples' the microstructure. In the present experiments where the small-crack dimensions were comparable with characteristic microstructural size-scales, their crack fronts cannot sample the 'continuum' microstructure. For example, whereas the average short crack in the bimodal microstructure would 'sample' some 300 grains, the small crack merely 'samples' one or two grains. Data on the behaviour of such cracks under mixed-mode loading are extremely limited although present results for the bimodal structure, at $R = 0.1$ only, are shown in Fig. 13 and are compared with the corresponding large- and short-crack mixed-mode threshold values. Clearly, the additional effect of microstructural sampling is evident in these results in which the small-crack thresholds can be seen to be lower than the corresponding values for short cracks and shielding-corrected large cracks. While the marked effect of crack size on the mixed-mode thresholds up to now has been attributed to a difference in the magnitude of the crack-tip shielding, the even lower mixed-mode thresholds for microstructurally small cracks reflect this additional factor of the biased sampling of the 'weak links' in the microstructure by the small flaw. Indeed, quantitatively, large-crack mixed-mode ΔG_{TH} thresholds in the bimodal structure at high mode-mixities $\Delta K_{II}/\Delta K_I = 7.1$ can be some ~50–90 times larger than such measured small-crack thresholds.

Table 6 Thresholds obtained for short fatigue cracks in Ti-6Al-4V

	ΔG_{TH} (J/m^2)			$\Delta K_{eq,TH}$ (MPa$\sqrt{m}$)		
Mode-mixity	$R = 0.1$	$R = 0.5$	$R = 0.8$	$R = 0.1$	$R = 0.5$	$R = 0.8$
Bimodal microstructure:						
0°	72	66	59	2.9	2.8	2.7
26°	125	105	85	3.9	3.6	3.2
62°	72	64	52	2.9	2.8	2.5
82°	148	140	130	4.2	4.1	4.0
Lamellar microstructure:						
0°	159	110	96	4.4	3.6	3.4
26°	176	131	119	4.6	4.0	3.8
62°	180	142	121	4.7	4.1	3.8
82°	210	145	125	5.0	4.2	3.9

DISCUSSION

In the present study, we have examined how varying the microstructure can affect the mixed-mode fatigue crack growth thresholds in a Ti-6Al-4V alloy as a function of load ratio and mode-mixity. What has been found is that microstructure, mode-mixity and load ratio all can have a major influence on the value of the mixed-mode threshold, *but only in the presence of cracks large compared with*

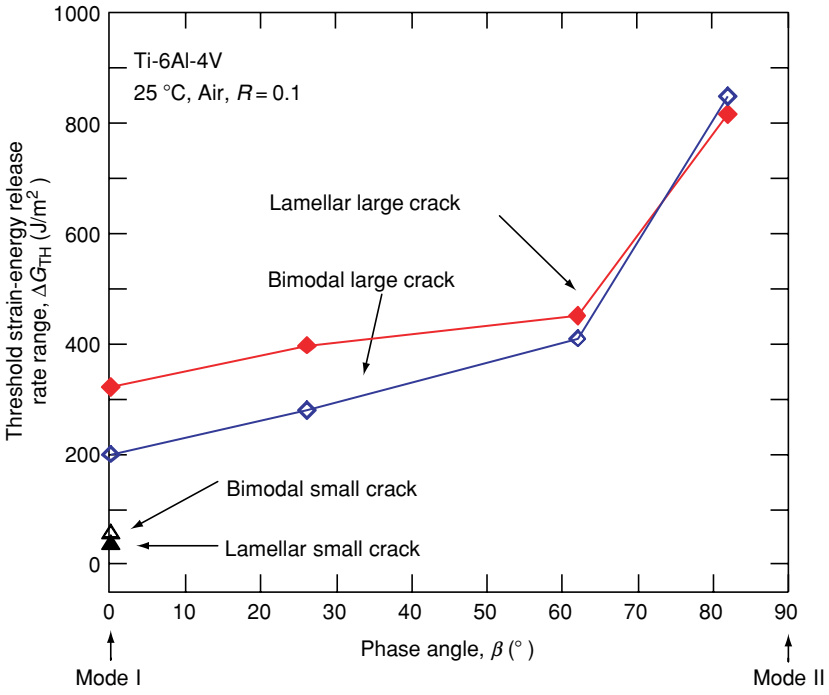

Fig. 11 Mixed-mode thresholds for large (> 4 mm) through-thickness fatigue cracks in bimodal and lamellar Ti-6Al-4V are compared with pure mode I thresholds for microstructurally small cracks. The superior resistance of the lamellar structure observed in the large crack regime is eliminated for small cracks, where the role of microstructural sampling becomes important.

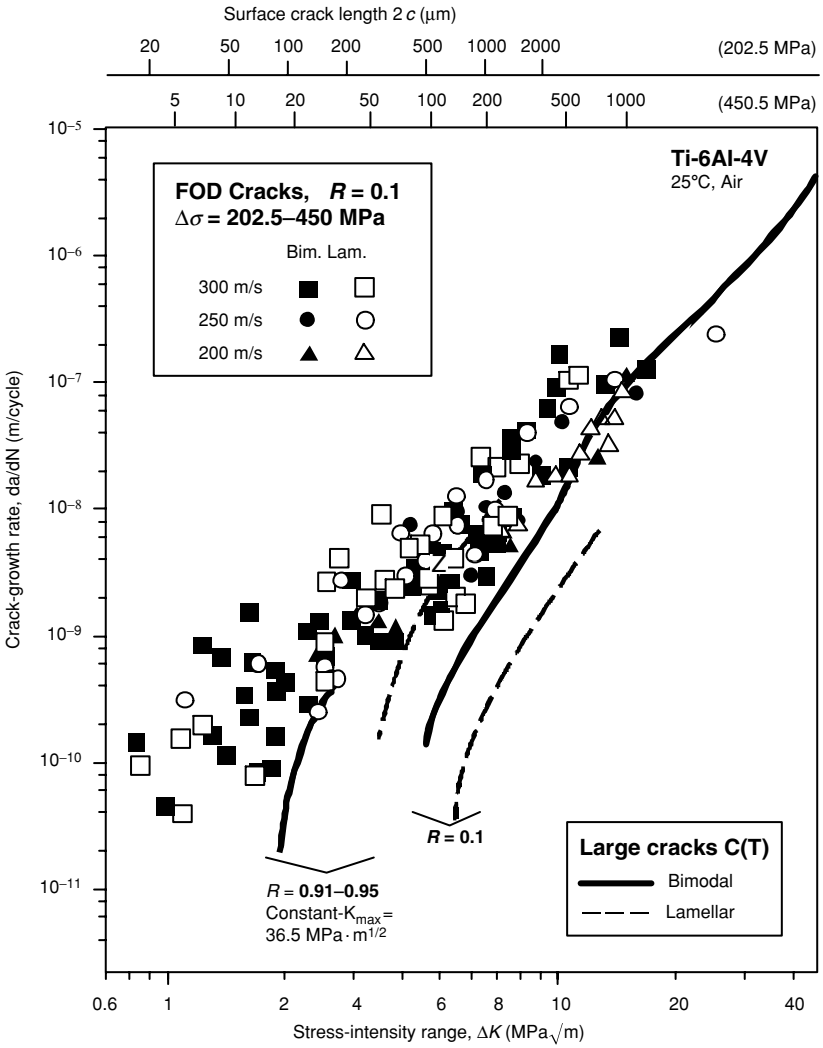

Fig. 12 Fatigue crack growth rates as a function of applied stress-intensity range at $R = 0.1$ for microstructurally small (~2–50 μm) surface cracks in the bimodal and lamellar microstructures. Large-crack growth data at $R = 0.1$ were obtained from constant load-ratio tests, whereas corresponding data at $R = 0.91$–0.95 were obtained using constant-K_{max}/increasing-K_{min} testing (after Ref. [42]).

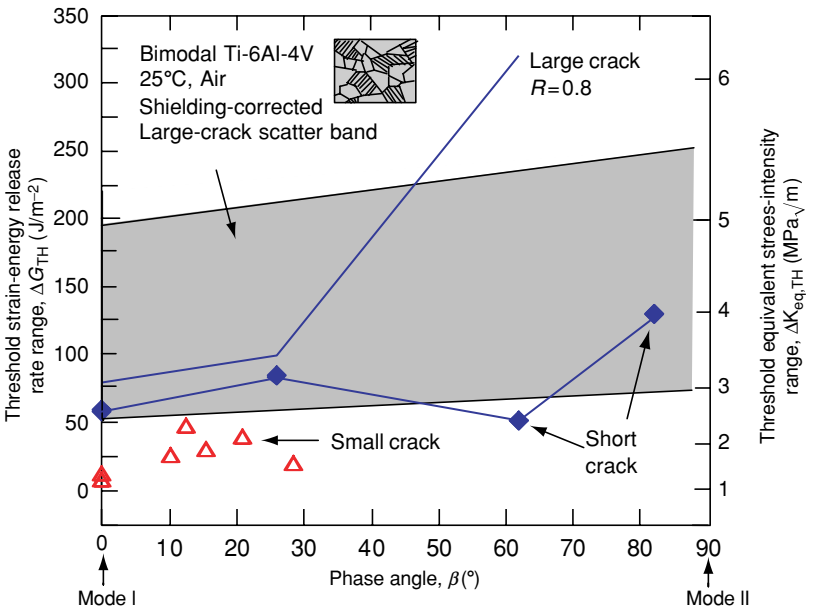

Fig. 13 Variation in mixed-mode thresholds, ΔG_{TH}, as a function of phase angle, β, for microstructurally small (< 50 μm) surface cracks in the bimodal microstructure. Shown for comparison are results for short (~200 μm) through-thickness cracks and for large (> 4 mm) through-thickness cracks under *worst-case*, high R conditions.

microstructural dimensions. The fact that microstructure, mode-mixity and load ratio all have a relatively insignificant effect on fatigue thresholds in the presence of short through-thickness cracks and microstructurally small surface cracks strongly implies a dominant role of crack-tip shielding dictated by crack path.

The superior crack-growth resistance, and hence higher large-crack ΔG_{TH} thresholds, in the lamellar structure appears to be a consequence of the preferential path taken by the propagating crack, which in turn promotes higher levels of crack-tip shielding. In aligned lamellar structures, the α phase is orientated perpendicular to the basal plane;[21] crack propagation parallel to the basal plane orientation is thus generally observed perpendicular to the orientation of the α laths.[22] Because the thin layer of β phase that surrounds the α laths cannot significantly alter the crack path, crack propagation invariably occurs with almost no change in direction through an entire colony of similarly orientated laths. This strongly crystallographic influence on the fatigue crack path is evident in the significant amount of out-of-plane deflection, secondary cracking and crack-path tortuosity that is characteristic of the coarser lamellar microstructures, as compared to the almost planar crack paths in the finer bimodal structures (Fig. 8).

Such microstructural factors can lead to two effects—one intrinsic and one extrinsic. In the coarser-grained lamellar structure, at the onset of the mixed-mode loading, the crack attempts to deviate along a direction different from that of the preferred path—that is, dictated by the $G_{\max}$, $K_{\mathrm{II}} = 0$ or maximum tensile stress (MTS) criteria. Although this clearly requires a higher driving force, its effect on the measured threshold is debatable because the crack is following a weaker *microstructural* path. More important though is the extrinsic effect in which the rougher crack paths give rise to the higher levels of crack closure and crack-surface interference, as shown, respectively, in Tables 4 and 5. The consequences of this are that because these mechanisms act in the crack wake, the prime effect of microstructure on the mixed-mode threshold arises from the presence of the precrack. Thus, as has been observed, it is to be expected that these microstructure effects will be far less apparent if the ΔG_{TH} thresholds are measured for short cracks.

A further point of note is that such beneficial effects of microstructure can only be developed where the crack front samples a large enough number of grains, as in the case of the large and short cracks examined in the present study. Indeed, where this is not the case—e.g. for microstructurally small cracks—this may lead to a reversal of the relative ranking of the two structures[21] although the present results do not show this too clearly (Fig. 11). The basis for this reversal involves the density of microstructural barriers that the crack front encounters. For large and short cracks, a large number of such barriers—e.g. grain boundaries, interfaces between dissimilarly orientated colonies, etc.—are encountered, leading to frequent changes in path, and hence increased tortuosity and higher thresholds for the lamellar structure. However, for small cracks, comparable in size to the characteristic microstructural size-scales, the crack front may encounter as few as one or two grains, or in the case of the lamellar structure be contained within a single grain, resulting in the crack front sampling a much lower density of barriers to crack propagation. Consequently, despite their superior large-crack properties, lamellar structures can show poorer resistance to fatigue crack propagation than bimodal structures in the small-crack regime.[21]

Finally, it is apparent that the near-elimination of the effect of mode-mixity on the large-crack ΔG_{TH} thresholds when crack-tip shielding is accounted for (either by measurement or by removal of the crack wake), strongly implies that the threshold behaviour of fatigue cracks under mixed-mode loading is predominantly a mode I phenomenon. The principal influence of the applied shear loading appears to be in dictating the crack-path deflection, in conjunction with the near-tip microstructure in the coarser microstructures; once the crack path is set by the phase angle, the initial crack extension and hence the mixed-mode threshold are dictated by the effective crack-driving force, which is largely independent of mode-mixity. The implications for this are that the mixed-mode fatigue threshold behaviour is essentially identical to mode I behaviour if the additional contributions to the crack-tip shielding that are induced owing to a deflected crack path are carefully accounted for. Moreover, it further implies that the ΔG_{TH} threshold, measured under pure mode I loading, can be considered to be a lower bound.

CONCLUSIONS

Based on an investigation of the mixed-mode high-cycle fatigue behaviour of the fine bimodal microstructure (grain size $\sim$20 μm) and the coarser lamellar microstructure (colony size $\sim$500 μm) in a Ti-6Al-4V turbine-engine alloy, the following conclusions can be made:

1. Both microstructures displayed a marked effect of mode-mixity and load ratio on the measured mixed-mode fatigue thresholds for through-thickness large ($>$4 mm) cracks. By characterizing the crack-driving force in terms of the strain-energy release rate, ΔG, the mode I threshold was found to represent the *worst-case* condition.
2. The coarse-grained lamellar microstructure was generally observed to have higher thresholds, and hence superior mixed-mode, near-threshold fatigue crack-growth

resistance, compared to the bimodal structure, in the presence of large through-thickness fatigue cracks. However, this difference was significantly reduced at high phase angles.

3 The marked effect of load ratio and mode-mixity was substantially reduced when the large-crack ΔG_{TH} thresholds were 'corrected' for crack-tip shielding owing to mode I crack closure and mode II crack-surface interference. As such shielding was promoted in the coarser lamellar microstructure by a higher degree of crack-path tortuosity and fracture-surface roughness, the superior large-crack properties of this structure were significantly reduced by such corrections.

4 Mixed-mode ΔG_{TH} thresholds for through-thickness short cracks ($\sim$200 μm) were substantially lower than corresponding large-crack thresholds in both microstructures; moreover, short-crack threshold values were essentially insensitive to load ratio and mode-mixity.

5 Compared to large-crack threshold behaviour, the influence of microstructure on such short-crack mixed-mode ΔG_{TH} thresholds was substantially reduced. This was attributed to the absence of crack-tip shielding effects with cracks of limited wake.

6 Results for naturally initiated microstructurally small (< 50 μm) semielliptical surface cracks in the bimodal microstructure indicate that mixed-mode ΔG_{TH} thresholds for such cracks are substantially lower than those for large cracks; indeed, large-crack thresholds at high mode-mixities ($\Delta K_{II}/\Delta K_I \sim 7.1$) can be some 50–90 times larger than such measured small-crack thresholds. The substantially lower small-crack thresholds were associated with a limited role of crack-tip shielding and additionally with biased microstructural sampling by cracks of a dimension comparable with the characteristic microstructural size-scales.

7 The prime source of the influence of mixed-mode loading in dictating the value of the mixed-mode ΔG_{TH} threshold is considered to arise primarily from the trajectory of the precrack. Because microstructure can influence this trajectory, in general microstructural effects on mixed-mode thresholds result mainly from the role of crack-tip shielding that arises from such crack paths. Where crack sizes are small enough so that such shielding cannot fully develop, the influence of microstructure on mixed-mode thresholds becomes minimal.

Acknowledgements

This work was supported by the US Air Force Office of Scientific Research under Grant No. F49620-96-1-0478 under the auspices of the Multidisciplinary University Research Initiative on *High-Cycle Fatigue* to the University of California at Berkeley. Special thanks are due to Drs B. L. Boyce, I. Altenberger, J. O. Peters and A. W. Thompson for helpful discussions.

REFERENCES

1 Report of the AdHoc Committee on Air Force Aircraft Jet Engine Manufacturing and Production Processes (1992) United States Air Force Scientific Advisory Board, SAF/AQQS: the Pentagon, Washington, D.C., USA.
2 Cowles, B. A. (1996) High-cycle fatigue in aircraft gas turbines – an industry perspective. *Int. J. Fract.* **80**, 147–163.
3 Chang, J. C. I. (1996) An integrated research approach to attack engine HCF Problems. Air Force Office of Scientific Research, Bolling AFB, Washington, D.C., USA.
4 Multidisciplinary University Research Initiative on High-Cycle Fatigue. Grant no. F49620–96–1–0478, U.S. Air Force Office of Scientific Research.
5 Waterhouse, R. B. and Lindley, T. C. (1994) *Fretting Fatigue* (Edited by European Structural Integrity Society Publication no. 18). Mechanical Engineering Publications Ltd, London, UK.
6 Iida, S. and Kobayashi, A. S. (1969) Crack-propagation rate in 7075-T6 plates under cyclic tensile and transverse shear loadings. *J. Bas. Eng. Trans. ASME* **91**, 764–769.
7 Gao, H., Alagok, N., Brown, M. W. and Miller K. J. (1985) Growth of fatigue cracks under combined mode I and mode II loads. In: *Multiaxial Fatigue*, ASTM STP 853 (Edited by K. J. Miller and M. W. Brown). ASTM, Philadelphia, PA, USA, pp. 184–202.
8 Pustejovsky, M. A. (1979) Fatigue crack propagation in titanium under general in-plane loading. I. Experiments. *Eng. Fract. Mech.* **11**, 9–15.
9 Pustejovsky, M. A. (1979) Fatigue crack propagation in titanium under general in-plane loading. II. Analysis. *Eng. Fract. Mech.* **11**, 17–31.
10 Campbell, J. P. and Ritchie, R. O. (2000) Mixed-mode, high-cycle fatigue-crack growth thresholds in Ti-6Al-4V. I. a comparison of large- and short-crack behavior. *Eng. Fract. Mech.* **67**, 209–227.
11 Campbell, J. P. and Ritchie, R. O. (2000) Mixed-mode, high-cycle fatigue-crack growth thresholds in Ti-6Al-4V. II. quantification of crack-tip shielding. *Eng. Fract. Mech.* **67**, 229–249.
12 Campbell, J. P. and Ritchie, R. O. (2001) Mixed-mode, high-cycle fatigue-crack growth thresholds in Ti-6Al-4V: role of bimodal and lamellar microstructures. *Metall. Mater. Trans. A* **32A**, 497–503.
13 Kruzic, J. J., Campbell, J. P. and Ritchie, R. O. (1999) On the fatigue behavior of γ-based titanium aluminides: role of small cracks. *Acta. Mater.* **47**, 801–816.
14 Thompson A.W. (1999) Relations between microstructure and fatigue properties of alpha–beta titanium alloys. In: *Fatigue Behavior of Titanium Alloys* (Edited by R. R. Boyer, D. Eylon and G. Lütjering). TMS, Warrendale, PA, USA, pp. 23–30.
15 Lütjering, G. (1998) Influence of Processing on Microstructure and Mechanical Properties of (α+β) Titanium Alloys. *Mater. Sci. Eng.* **A243**, 32–45.
16 Irving, P. E. and Beevers, C. J. (1974) Microstructural influences on fatigue crack growth in Ti-6Al-4V. *Mater. Sci. Eng.* **14**, 229–238.
17 Bache, M. R., Evans, W. J. and McElhone, M. (1997) The effects of environment and internal oxygen on fatigue crack propagation in Ti-6Al-4V. *Mater. Sci. Eng.* **A234–236**, 918–922.
18 Thomas, J. P. (1998) Subcritical crack growth of Ti-6Al-4V at room temperature under high stress-ratio loading. *Scripta Mater.* **39**, 1647–1652.

19 Ravichandran, K. S. (1991) Near threshold fatigue crack growth behavior of a titanium alloy: Ti-6Al-4V. *Acta Metall. Mater.* **39**, 401–410.
20 Boyce, B. L. and Ritchie, R. O. (2001) Effect of load ratio and maximum stress intensity on the fatigue threshold in Ti-6Al-4V. *Eng. Fract. Mech.* **68**, 129–147.
21 Gregory, J. K. (1994) Fatigue crack propagation in titanium alloys. In: *Handbook of Fatigue Crack Propagation in Metallic Structures* (Edited by A. Carpinteri). Elsevier Science B, V., Amsterdam, The Netherlands, pp.281–321.
22 Nalla, R. K., Boyce, B. L., Campbell, J. P., Peters, J. O. and Ritchie, R. O. (2002) Influence of microstructure on high-cycle fatigue of Ti-6Al-4V: bimodal vs. lamellar structures. *Metall. Mater. Trans. A* **33A**, 899–918.
23 Eylon, D. (1998) Summary of available information on the processing of the Ti-6Al-4V HCF/LCF program plates. University of Dayton Report, Dayton, OH, USA.
24 Boyce, B. L. (1998) High Cycle Fatigue Thresholds in a Turbine Engine Titanium Alloy. *MSc Thesis*, University of California at Berkeley, Berkeley, CA, USA.
25 He, M. Y., Cao, H. C. and Evans, A. G. (1990) Mixed-mode fracture: the four-point shear specimen. *Acta Metall. Mater.* **38**, 839–846.
26 Suresh, S., Shih, C. F., Morrone, A., O'Dowd, N. P. (1990) Mixed-mode fracture toughness of ceramic materials. *J. Am. Ceram. Soc.* **73**, 1257–1267.
27 Slepetz, M., Zagaeski, T. F. and Novello, R. F. (1978) AMMRC-TR-78-30, Army Materials and Mechanics Research Center, Watertown, MA, USA.
28 He, M. Y. and Hutchinson, J. W. (2000) Asymmetric four-point crack specimen. *J. Appl. Mech. Trans. ASME* **67**, 207–209.
29 Newman, J. C. and Raju, I. S. (1981) An empirical stress-intensity factor equation for the surface crack. *Eng. Fract. Mech.* **15**, 185–192.
30 He, M. Y. and Hutchinson, J. W. (2000) Surface crack subject to mixed mode loading. *Eng. Fract. Mech.* **65**, 1–14.
31 Ravichandran, K. S. (1997) Effects of crack aspect ratio on the behavior of small surface cracks in fatigue: Part I. simulation. *Metall. Mater. Trans. A* **28A**, 149–156.
32 Ravichandran, K. S. and Larsen, J. M. (1997) Effects of crack aspect ratio on the behavior of small surface cracks in fatigue: Part II. experiments on a titanium (Ti-8Al) alloy. *Metall. Mater. Trans. A* **28A**, 157–169.
33 Hua, G., Brown, M. W. and Miller, K. J. (1982) Mixed-mode fatigue thresholds. *Fat. Eng. Mater. Struct.* **5**, 1–17.
34 Tong, J., Yates, J. R. and Brown, M. W. (1994) The significance of mean stress on the fatigue crack growth threshold for mixed mode I + II loading. *Fat. Eng. Mat. Struct.* **17**, 829–838.
35 Qian, J. and Fatemi, A. (1996) Mixed mode fatigue crack growth: a literature survey. *Eng. Fract. Mech.* **55**, 969–990.
36 Erdogan, F. and Sih, G. C. (1963) On the crack extension in plates under plane loading and transverse shear. *J. Bas. Eng. Trans. ASME* **85**, 519–525.
37 Cotterell, B. (1965) On brittle fracture paths. *Int. J. Fract. Mech.* **1**, 96–103.
38 John, R., Rosenberger, A. H., DeLuca, D., Porter J. W. and Li, K. (1999) Mixed mode crack growth in a gamma titanium aluminide alloy. In: *Gamma Titanium Aluminides 1999* (Edited by Y. W. Kim, D. M. Dimiduk and M. H. Loretto). TMS, Warrendale, PA, USA, pp. 535–540.
39 Nayeb-Hashemi, H., McClintock, F. A. and Ritchie, R. O. (1982) Effects of friction and high torque on fatigue crack propagation in mode III. *Metall. Trans. A* **13A**, 2197–2204.
40 Tschegg, E. K. (1983) Sliding mode crack closure and mode III fatigue crack growth in mild steel. *Acta Metall.* **31**, 1323–1330.
41 Zheng, Y. S., Wang, Z. G. and Ai, S. H. (1994) Mixed-mode I and II fatigue threshold and crack closure in dual-phase steels. *Metall. Mater. Trans. A* **25A**, 1713–1723.
42 Peters, J. O. and Ritchie, R. O. (2001) Foreign object damage and high cycle fatigue: Role of microstructure in Ti-6Al-4V. *Int. J. Fatigue* **23**, 1413–1421.
43 Suresh, S. and Ritchie, R. O. (1984) Propagation of short cracks. *Int. Metals. Rev.* **29**, 445–476.
44 Ritchie, R. O. and Lankford, J. (1986) Small fatigue cracks: a statement of the problem and potential solutions. *Mater. Sci. Eng.* **A84**, 11–16.
45 Ritchie R.O. and Wu Y. (1986) Short crack effects in fatigue: a consequence of crack tip shielding. In: *Small Fatigue Cracks* (Edited by R. O. Ritchie and J. Lankford.). TMS-AIME, Warrendale, PA, USA, pp. 167–189.
46 Venkateswara Rao, K. T., Yu, W. and Ritchie, R. O. (1988) On the behavior of small fatigue cracks in commercial aluminum–-lithium alloys. *Eng. Fract. Mech.* **31**, 623–635.
47 Bilby, B. A., Cardew, G. E. and Howard, I. C. (1978) Stress intensity factors at the tips of kinked and forked cracks. In: *Fracture 1977* (Edited by D. M. R. Taplin), Pergamon Press, Oxford. U.K., Vol. 3, pp. 197–200.
48 Cotterell, B. and Rice, J. R. (1980) Slightly curved or kinked cracks. *Int. J. Fract.* **16**, 155–169.
49 Nalla, R. K., Campbell, J. P. and Ritchie, R. O. (2002) Mixed-mode, high-cycle fatigue-crack growth thresholds in Ti-6Al-4V: role of small cracks. *Int. J. Fatigue*, in press.

APPENDIX A

Distinction between large, short and small cracks

A point of note in this work is the distinction between *large*, *short* and *small* cracks. Large fatigue cracks (Fig. A1a) are defined as having dimensions that are large compared to the scale of the microstructure in both directions. Therefore, they generally have a fully developed crack-tip shielding zone and can 'sample' the microstructure in a statistical (continuum) manner.[43] With respect to large cracks, small cracks are generally described as being comparable in size to:[44]

- microstructural dimensions, where biased statistical sampling of the microstructure can lead to accelerated crack advance along 'weak' paths; that is, microstructural features orientated for easy crack growth (a continuum limitation),
- the extent of local inelasticity *ahead* of the crack tip, where the assumption of small-scale yielding implicit in the use of the stress intensity, K, is not strictly valid (a linear-elastic fracture mechanics limitation),
- the extent of crack-tip shielding (e.g. crack closure) *behind* the crack tip, where the reduced role of shielding leads to

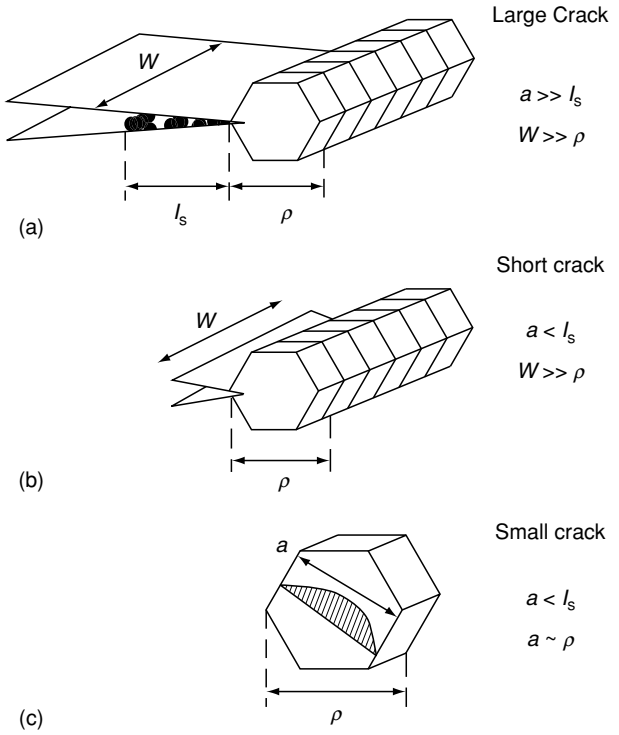

Fig. A1 Schematic illustrations highlighting the key distinctions between large, short and small fatigue cracks. Large cracks (a) have length, a, and width, W, which are large both with respect to the equilibrium shielding-zone length, l_s (indicated here as a region of debris in the crack wake which produces crack closure), and the characteristic microstructural size scale, ρ, e.g. the grain size. In contrast to this, short fatigue cracks (b) are characterized by a $< l_s$, but $W \gg \rho$. The reduced crack-wake length results in a lower level of crack-tip shielding. For small cracks (c), the fracture surface is reduced in both dimensions, with a (and W) being small with respect to both l_s and ρ. The fact that $a \sim \rho$ implies that the crack front samples only a few microstructural entities, leading to a biased sampling of the microstructure.

a higher local driving force than the corresponding large crack at the same applied K level (a similitude limitation).

However, a further important distinction can be made, namely that of a short vs. small crack. This distinction alludes not simply to physical size but the extent to which a fatigue crack is subjected to the first and third factors listed above. Short fatigue cracks (Fig. A1b) are physically short in only one dimension, a condition that is often realized experimentally by machining away the wake of a large crack. This type of fatigue flaw experiences limited crack-tip shielding owing to its reduced length,[45] yet samples the microstructure as a continuum because of its extensive crack front. By contrast, small fatigue cracks (Fig. A1c) are small and comparable to the microstructural size-scale in all dimensions, as typified by the small, semielliptical surface flaw (e.g. Refs [44,46]). With such cracks, crack-tip shielding is significantly reduced (e.g. Ref. [43]), and since the crack front samples only a few microstructural entities, this allows for a biased sampling of microstructurally weak paths. Because of this restriction in shielding and the biased microstructural sampling, fatigue crack growth resistance in the presence of small cracks often tends to be lowest.

Appendix B

Calculation of the mixed-mode threshold

In this work, as in prior studies (e.g. Refs [7–12,33,34]) on mixed-mode fatigue thresholds, the threshold values of the mode I and mode II stress intensities required to initiate cracking, $\Delta K_{I,TH}$ and $\Delta K_{II,TH}$, are calculated based on the mode I precrack (which is generated in near-identical fashion for each test); the corresponding mixed-mode threshold, ΔG_{TH}, or equivalent stress intensity, $\Delta K_{eq,TH}$, are then computed from:

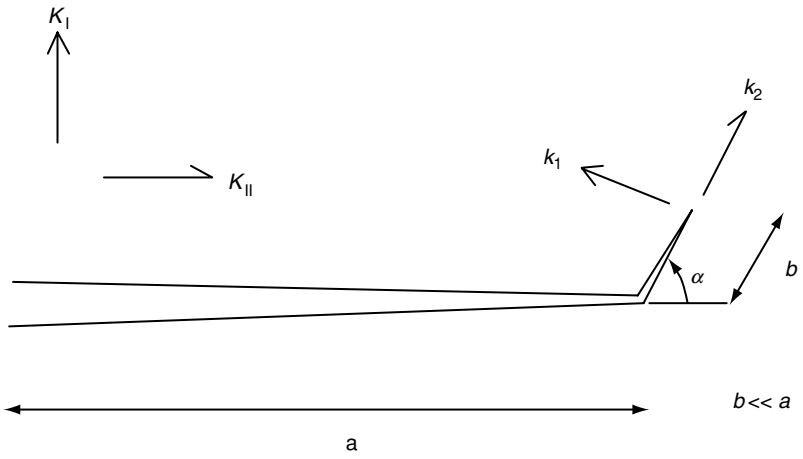

Fig. A2 Schematic illustration of the kinked crack configuration for the alternative calculation of the mixed-mode threshold.

$$\Delta G_{TH} = \left(\Delta K_{I,TH}{}^2 + \Delta K_{II,TH}{}^2\right)/E'^1 \equiv \left(\Delta K_{eq,TH}{}^2\right)/E' \quad \text{(A1)}$$

where E' is the appropriate elastic modulus.

However, since once the crack starts to grow, it deflects along a different path (corresponding to a local $K_{II} = 0$ criterion modified by the effect of the microstructure), an alternative calculation of the threshold can be based on the presence of an infinitesimal kink along this direction. Assuming for simplicity that the kink (of length $b << a$, the crack length) represents an in-plane tilt through angle α to the precrack plane (Fig. A2), then the local mode I and mode II stress intensities, Δk_1 and Δk_2, at the deflected crack tip will be given by:[47,48]

$$\begin{aligned} \Delta k_1(\alpha) &= c_{11}\Delta K_I + c_{12}\Delta K_{II} \\ \Delta k_2(\alpha) &= c_{21}\Delta K_I + c_{22}\Delta K_{II} \end{aligned} \quad \text{(A2)}$$

where ΔK_I and ΔK_{II} are the stress intensities for a main (pre)crack, and the coefficients c_{ij}, which are a sole function of α, are given in Refs [47,48]. The mixed-mode thresholds, $\Delta G'_{TH}$ and $\Delta K'_{TH}$, can then be computed from:

$$\Delta G'_{TH} = \left(\Delta k_{1,TH}{}^2 + \Delta k_{2,TH}{}^2\right)/E' \equiv \left(\Delta K'_{TH}{}^2\right)/E' \quad \text{(A3)}$$

As discussed elsewhere,[49] the use of Eqn. A3 to calculate the mixed-mode threshold can in fact reduce the computed values of $\Delta K_{eq,TH}$, at specific phase angles by as much as 40%. For the bimodal and lamellar Ti-6Al-4V, this translates into a reduction in threshold $\Delta K_{eq,TH}$ values by typically 1–2 MPa$\sqrt{}$m.